Article

Degradation Effect of Moisture on Mechanical Properties of Kevlar/PVB Composites with TiO₂ Nanoparticles

Vera Obradović [1,2,*] , Petr Sejkot [2] , Adam Zabloudil [2] , Klára V. Machalická [2] and Miroslav Vokáč [2]

[1] Innovation Center of Faculty of Technology and Metallurgy in Belgrade, 4, Karnegijeva Street, 11120 Belgrade, Serbia

[2] Klokner Institute, Czech Technical University in Prague, Šolínova 7, 166 08 Prague, Czech Republic; petr.sejkot@cvut.cz (P.S.); adam.zabloudil@cvut.cz (A.Z.); klara.machalicka@cvut.cz (K.V.M.); miroslav.vokac@cvut.cz (M.V.)

* Correspondence: vera.obradovic@cvut.cz

Abstract: Kevlar fibers are widely used for industrial and military purposes due to their remarkable mechanical properties, such as their high tenacity and high strength-to-weight ratio. In this study, two-layered Kevlar composite specimens were impregnated with 10 wt.% poly (vinyl butyral)/ethanol solution which contained TiO₂ nanoparticles as reinforcement. The concentrations of the nanoparticles were 1 wt.% or 2 wt.% with respect to the poly (vinyl butyral), PVB. The single-axial tensile test and three-point bending test of the Kevlar/PVB composites have been performed according to the ASTM D 3039 and ASTM D 790-03 standards, respectively. The tensile and bending properties of the dry and wet Kevlar/PVB composite specimens after a 56-day immersion are examined in this work. Upon the addition of the 2 wt.% TiO₂ nanoparticles, the tensile strength and modulus of the dry specimens without reinforcement were increased by 39.8% and 24.3%, respectively. All the submerged specimens' tensile and flexural property values were lower than those of the dry specimens. After comparing the wet composite specimens to their dry counterparts, the percentage decrease in tensile strength was approximately 20%. The wet Kevlar/PVB specimens with no TiO₂ reinforcement showed the greatest reduction in bending strength, 61.4% less than for the dry Kevlar/PVB specimens, due to the degradation of the PVB matrix. In addition, a numerical simulation of the three-point bending test was carried out in Abaqus.

Keywords: Kevlar/PVB composites; TiO₂ nanoparticles; water immersion; degradation effect; tensile test; bending test; FTIR analysis; numerical modelling

1. Introduction

Woven or multiaxial textiles made from para-aramid (poly (p-phenylene terephthalamide), PPTA) fibers are an excellent choice for soft body armor and lightweight vehicle armor structures. These textiles are often impregnated with different thermosetting resins or thermoplastic polymers. Kevlar, Twaron, and Kolon are para-aramid fibers, and they are synthetic fibers of high performance with a high strength-to-weight ratio, exceptional impact resistance, outstanding thermal stability, low flammability, high chemical resistance, and high tensile strength. Additionally, they are used for fireproof clothing, high-strength ropes, tyre cords, boat hulls, and sporting goods [1,2]. Kevlar, like any other fiber of the aramid group, consists of long-molecular-chain PPTA polymers which are reinforced and connected by van der Waals forces, hydrogen bonds, and π–π stacking bonds among themselves. For this reason, Kevlar fibers have exceptional mechanical properties. The longitudinal tensile qualities of Kevlar fibers are desired but these fibers have insufficient compressive strength. Owing to their anisotropic nature, Kevlar fiber composites have a very high ratio of tensile to compression strength. However, these composites have some excellent impact qualities because of their ability to absorb increased impact energy, which is further dispersed in the form of plastic deformation. Kevlar fibers are widely employed

in industrial and military applications as innovative composite materials for aircrafts and automotive manufacturing because of their remarkable mechanical properties [3,4]. They have even been used in acrylic dentures for better fatigue and fracture resistance [5].

The condensation of poly (vinyl alcohol) (PVA) and n-butyraldehyde in an acidic environment produces poly (vinyl butyral), or PVB, which is a thermoplastic polymer. Hydrophobic vinyl butyral groups and hydrophilic vinyl alcohol groups are present in PVB. This low-cost polymer is utilized in a variety of industrial applications, primarily in the automotive and aerospace industries. It is also widely used as an interlayer in the fabrication of laminated glass structures, in coatings and composites for ballistic protection. PVB is renowned for its great adhesive properties when mixed with different materials, such as glass, metal, plastics, and wood. It is characterized by a high impact strength at low temperatures, great elasticity and flexibility, excellent freezing and aging resistance, high compatibility with organic solvents, and high optical transparency. PVB is easily soluble in alcohols, as well as in many other organic solvents (methanol, ethanol, n-butanol, acetone, chloroform, etc.). Apart from being transparent and non-toxic, PVB has good film formation properties due to its strong binding, quick drying, and rapid solvent release [6–12].

Recent research has demonstrated that the mechanical properties of composite structures can be significantly improved by adding nanoscale reinforcement to the polymer matrix [6,13]. Nanomaterials are employed as reinforcement in polymer matrices because they display both extremely high stiffness and hardness. Small additions of nanoparticles (1 wt.%) may improve the mechanical properties of the matrices. Both organic and inorganic materials can be used as fillers or reinforcement in polymeric systems. Nanomaterials that are most frequently used in improving the properties of polymers are ceramics (TiO_2, SiO_2, Al_2O_3, etc.), carbon nanotubes, carbon fibers, nanodiamonds, fullerene, and metals (Ag, Au, Pt, Fe, etc.). Generally, the incorporation of ceramic nanoparticles not only increases the mechanical and thermal stability of the polymer matrices, but also gives rise to some additional functions that depend on the chemical composition and structure of the ceramic nanofillers. Titanium dioxide (TiO_2) is found in nature in three polymorphous forms: anatase, tetragonal rutile, and rhombic brookite. It is non-hygroscopic and does not dissolve in water. The different properties of TiO_2 nanoparticles depend on their synthesis method, morphology, crystalline structure, and crystallite size. Titanium dioxide nanoparticles are the most utilized ceramic nanoreinforcement because of their small particle size, high surface area, ease of processing, and capacity to exist in various forms, such as nanotubes, nanowires, nanoribbons, etc. The benefits of TiO_2 nanoparticles include chemical inertness, non-toxicity, low cost, commercial availability, corrosion resistance, and broad-spectrum UV filtering abilities. These nanoparticles are used in solar cells, optical devices, gas sensors, waste water purification, plastic additives, lithium battery electrode materials, the photocatalytic destruction of bacteria, etc. Polymer/TiO_2 nanocomposites have already been developed in many different applications as the quality of these nanoparticles is easily adjustable. Numerous polymers, including thermoplastic, thermosetting, and conductive ones, use TiO_2 as a filler ingredient. The mechanical, thermal, optical, and electrical properties of thermoplastic polymers could be enhanced by a small amount of TiO_2 nanofillers [14–18].

The mechanical characteristics of fiber-reinforced composites with an organic matrix degrade in humid surroundings because they absorb moisture. Both the PVB matrix and Kevlar fibers absorb water [19,20]. The interfaces between the fiber and the epoxy matrix are essential for the transfer of stress in composite materials, but moisture absorption can have an impact on them [21]. In most composites, matrix plasticization or the deterioration of the fiber/matrix interface is supposed to be caused by moisture [2].

There is a lack of literature on the moisture properties of Kevlar composites with TiO_2 nanoparticles. This work examines the influence of TiO_2 nanoparticles and an 8-week immersion on the mechanical characteristics of Kevlar/PVB composites. The aim of this research is to present a comparison of the tensile and bending test results of dry and water-immersed Kevlar/PVB composite specimens.

2. Materials and Methods

2.1. Materials

The 10 wt.% PVB solution was prepared with PVB powder (Mowital B60H, Kuraray Specialities Europe, Holešov–Všetuly, Czech Republic) and ethanol (95%, Nanolab, Brno, Czech Republic). The composites were produced using Kevlar textiles (Woven Aramid Style 1350, 470 g/m^2 format Panama 4/4).

As reinforcement, TiO$_2$ nanoparticles (nanopowder, 21 nm primary particle size, Sigma Aldrich, Prague, Czech Republic) were added to the PVB solution.

2.2. Preparation of the Samples

The 10 wt.% PVB solutions with the TiO$_2$ nanoparticles used for the impregnation of the Kevlar fabrics were prepared by first adding the nanoparticles, at a concentration of either 1 wt.% or 2 wt.% with regard to PVB, to the ethanol on a magnetic stirrer. Next, the PVB powder was gently mixed with the same ethanol and stirred constantly until it was dissolved.

For the Kevlar fabric impregnation, the weight ratio of PVB to fabric was 20 wt.%. All the composite samples comprised two layers of impregnated fabrics. These layers were heated to 170 °C for 30 min in a heat press machine (Yiwu Sunmeta Technology Co., Ltd., ST-4050 model, Yiwu City, province Zhejiang, China)—Figure 1. Three types of composite samples were produced: the No. 1-Kevlar/PVB, No. 2-Kevlar/PVB/1% TiO$_2$, and No. 3-Kevlar/PVB/2% TiO$_2$ samples.

| (a) | (b) |
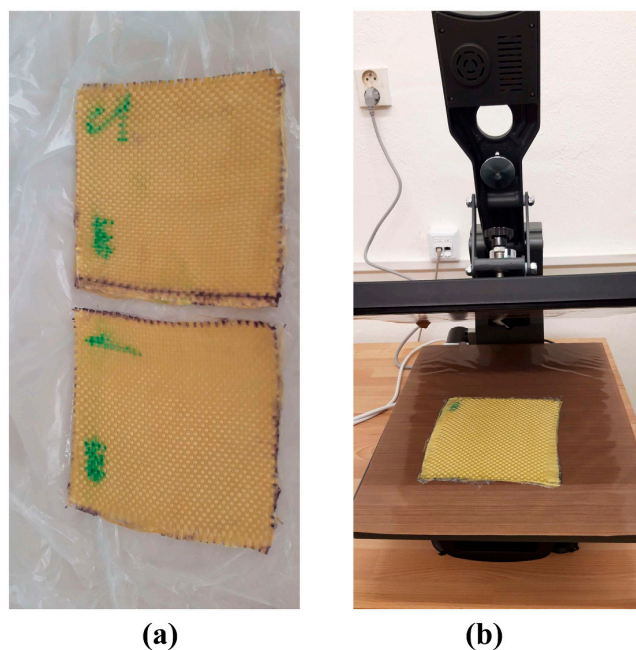
Figure 1. Preparation of the Kevlar/PVB composites: (**a**) impregnated Kevlar fabric layers and (**b**) fabrication of the two-layered Kevlar composite sample.

The specimens that were cut from the Kevlar/PVB composite samples had the following dimensions: 200 mm × 15 mm for the tensile test, and 50.8 mm × 15 mm for the bending test. Additionally, the square specimens measuring 50 mm by 50 mm were cut out for the measurements of water absorption. All of the specimens were approximately 1 mm thick.

2.3. Characterization

For the water gain measurements, the square specimens were dried in an oven at 50°C in compliance with the ISO 62 standard [22] before being submerged in water. The specimens were immersed in a water bath (GFL 1008) filled with distilled water at a

temperature of 40 °C for 56 days (8 weeks). Subsequently, the weight of the square specimens was periodically determined using the KERN ALJ 250-4A analytical balance after their surface had been dried. The same bath and the same conditions were applied to the immersion of the specimens used for the tensile and the bending tests.

The following equation was used to determine the percentage of water absorption for the square specimens at various times:

$$M(t) = \left(\frac{w_t - w_0}{w_0} \right) \times 100 \tag{1}$$

where $M(t)$ is the water uptake percentage and w_t is the current weight at time t, while w_0 is the weight of dry fabric before the immersion, at $t = 0$ [23]. For each composite type, three square specimens were measured.

The FTIR spectroscopy of both the dry and wet square specimens was performed using a Nicolet iN10 microscope with an iZ10 ATR module (Thermo Fisher Scientific, Waltham, MA, USA) in the attenuated total reflection mode at 4 cm^{-1}. The spectra were taken in the wavelength range of 4000 cm^{-1} to 400 cm^{-1}.

The single-axial tensile test and the three-point bending test were carried out using the TIRA TEST 2300 testing machine (modernized by the TEMPOS company, Opava, Czech Republic, TIRA's representative in the Czech Republic) at room temperature (20 ± 2 °C) and relative humidity of 50 ± 10%. Each specimen for the tensile test measured 200 mm overall, and 130 mm between the clamps. In order to meet the ASTM D 3039 standard for the tensile properties of polymer composite materials [24], the cross-head displacement rate of 2 mm/min was used to test the Kevlar/PVB specimens. Four specimens per composite type were tested, and the 100 mm-long extensometer was used to measure the strain (Model 3542 by Epsilon Technology Corp., Jackson, MS, USA). Furthermore, field emission scanning electron microscopy (FE-SEM) was used to investigate the surfaces of the specimens using the Tescan Mira3 XMU electron microscope at 10 kV.

In accordance with the ASTM D 790-03 standard for flexural properties [25], the three-point bending test was conducted on the Kevlar/PVB specimens with a cross-head displacement rate of 1 mm/min. The span length was 25.4 mm and the thickness of specimens was 1 mm. Thus, the span-to-thickness ratio was 25.4. Five specimens for each composite type were examined.

The mechanical characterization devices for the tensile and bending tests are shown in Figure 2.

(a)   (b)
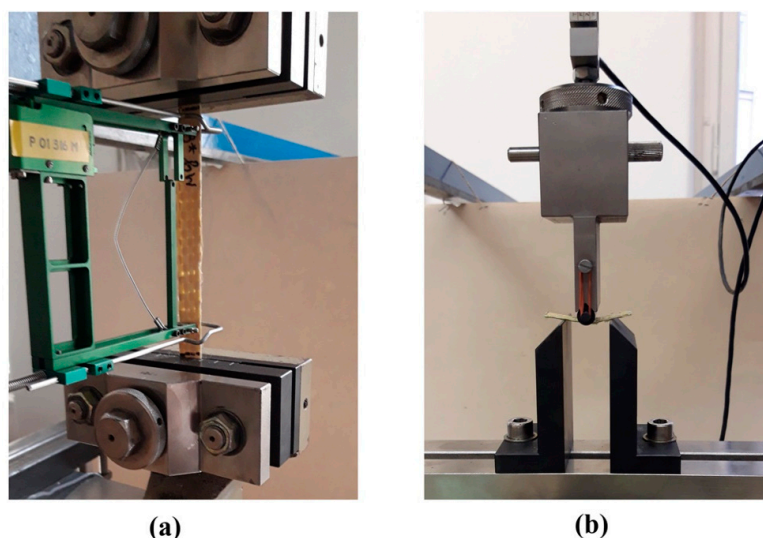
Figure 2. The TIRA TEST 2300 testing machine set-up for: (**a**) the tensile test and (**b**) the three-point bending test.

2.4. Numerical Modelling

A numerical simulation of the experimental testing was carried out in the Abaqus software (version 2021). The aim of this simulation is to study the influence of the nonlinear (second-order) effects on the calculation of the stress in the outer fibers at midpoint. Therefore, the "Nlgeom" setting was used in Abaqus in each step of the simulation to include nonlinear effects from large displacements and deformations.

3. Results and Discussion

3.1. Water Absorption Results

The main factors that affect the water absorption in fiber-reinforced composites are humidity, fiber volume fraction, void content, and temperature. Moreover, aramid fibers absorb water through the vacancies in their structure [2].

Figure 3 depicts the percentage of water uptake as a function of the immersion time for the three types of specimens. It can be noticed that the water uptake of the Kevlar/PVB specimens (No. 1 composite type) was the highest one (36.9%), while, for the other two types of specimens with TiO_2 nanoparticles, the absorption was lower, around 30.5% after 8 weeks of immersion. These results are in agreement with some findings that the water absorption of nanocomposites decreases as the nanoparticles make the barriers for the water molecules to extend in the composites [26,27].
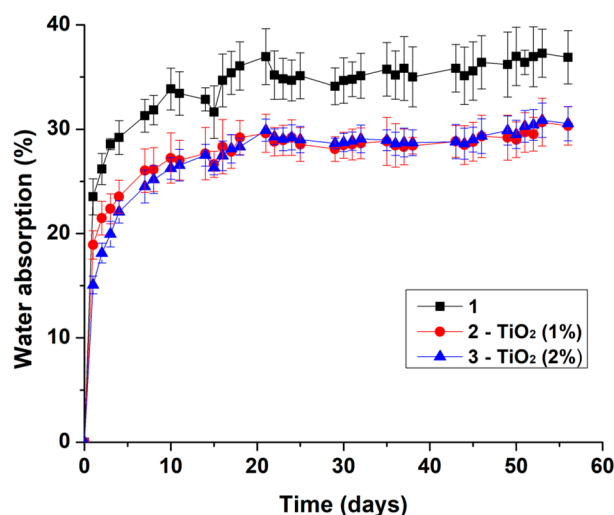

Figure 3. The water uptake of composites with their immersion time.

3.2. FTIR Analysis

Figure 4 shows the FTIR spectra of the dry and wet Kevlar/PVB/1% TiO_2 specimens.

For both of the specimens, the N-H stretching vibration was observed at 3317 cm^{-1}, while the peaks around 2870 cm^{-1}, 2920 cm^{-1}, and 1100 cm^{-1} corresponded to the stretching vibrations of the C-H groups. The peaks at 1637 cm^{-1} and 1379 cm^{-1} were related to the C=O groups and the Ti-O modes, respectively. The absorption bands at 995 cm^{-1} and 819 cm^{-1} were observed for the C-H groups of the aromatic structure. When the FTIR spectrum of the wet Kevlar/PVB/1% TiO_2 specimen is compared with the dry one, it can be seen that the peak intensity around 3317 cm^{-1} has increased because of the water-originated OH groups. The same result was detected with the peak at 1637 cm^{-1}, where the hydroxyl groups of water contributed to its enlargement [5,28,29]. The FTIR analysis indicated that the wet Kevlar/PVB composite specimen had hydrated and showed that some chemical changes had occurred during the immersion of that specimen as a result of the water absorption.
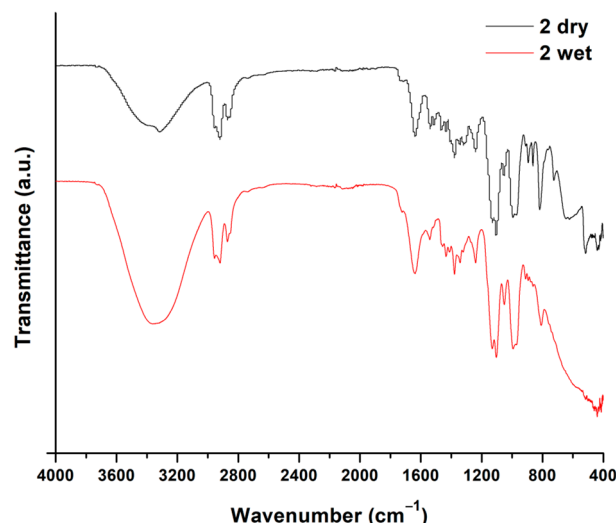
Figure 4. FTIR spectra of: dry and wet Kevlar/PVB/1% TiO$_2$ specimens.

3.3. Tensile Test Results

In the course of the tensile and bending tests, an incomplete rupture was caused in all the specimens. The specimens remained undamaged in the tensile testing machine's clamps, thus proving the test validity. At the time of the tensile test, the fracture of the Kevlar fibers and their pulling out occurred along with their elongation. The tensile energy absorption (TEA) was calculated as the area under the entire stress–strain diagram obtained with the extensometer, until the fracture point [30]. The inclusion of the 2 wt.% TiO$_2$ nanoparticles in the dry Kevlar/PVB specimens resulted in 39.8% and 24.3% improvements of the tensile strength and tensile modulus of these specimens, respectively, as shown in Table 1. These enhancements were expected because the stiffness of a composite can be increased by the addition of some inorganic nanoparticles with a higher rigidity than polymer matrices [31,32]. The polymer matrix is typically reinforced with nanofillers, since it must sustain high mechanical loads. Different fillers improve the stiffness of the material and may also increase its strength under specific load conditions [18].

Table 1. The tensile test results.

Specimen	Tensile Strength (MPa)	TEA (N/mm^2)	Tensile Modulus (GPa)
Kevlar/PVB—dry	369.71 ± 30.00	7.70 ± 2.65	24.85 ± 4.42
Kevlar/PVB—wet	293.09 ± 15.34	7.80 ± 0.47	19.02 ± 2.51
Kevlar/PVB/1% TiO$_2$—dry	423.80 ± 29.05	5.87 ± 1.53	23.15 ± 2.31
Kevlar/PVB/1% TiO$_2$—wet	351.41 ± 21.41	5.12 ± 2.43	22.02 ± 1.11
Kevlar/PVB/2% TiO$_2$—dry	516.84 ± 42.01	8.85 ± 2.99	30.90 ± 1.99
Kevlar/PVB/2% TiO$_2$—wet	426.03 ± 20.45	6.51 ± 1.47	25.98 ± 2.48

The tensile properties of the dry specimens and those that had been water-immersed were compared. Most organic polymers can be penetrated by water molecules, which changes their mechanical and chemical characteristics significantly. Plasticization, hydrolysis, and other forms of degradation are the main effects of the moisture absorption on the polymer itself, which results in both irreversible and reversible changes to the polymer's structure [33]. Water absorption in composites generally causes a decline in their mechanical characteristics due to fiber swelling and the disintegration of the fiber/matrix interface [23]. In this study, it also develops as a result of the hygroscopic Kevlar fiber [34]. This may help explain why the tensile strength and modulus values of all the immersed Kevlar/PVB composite specimens were slightly lower than those of their dry counterparts. Table 1 shows that the percentage decreases in tensile strength for the Kevlar/PVB,

Kevlar/PVB/1% TiO_2, and Kevlar/PVB/2% TiO_2 specimens that were immersed, as compared to their dry specimens, were 20.7%, 17.1%, and 17.6%, respectively. Similar trends were observed in the tensile modulus values of the same wet specimens, with percentage drops of 23.5%, 4.9%, and 15.9%, correspondingly, in comparison with their unprocessed specimens. The data obtained were also subjected to statistical analysis, especially with regard to the coefficient of variation (CoV). The results for the tensile strength can be considered to be the most reliable, as, in all cases, the CoV was below 10%. The results for the tensile modulus can also be considered to be very reliable, as the CoV is mostly below 10% and only two datasets exceed this value, but not beyond 18%. The least reliable results can be considered to be those determined from the test diagrams (stress–strain or force-displacement). These diagrams are characterized by considerable variability, which is also reflected in the CoV of the determined TEA values (CoV of up to 48%). Such values are expected for a composite material of this type, as the results are affected by the randomness of the fiber distribution in the fabric, variations in the geometry of the specimens, the test set-up, etc.

As examples, Figure 5 shows the stress versus strain plots from the extensometer.
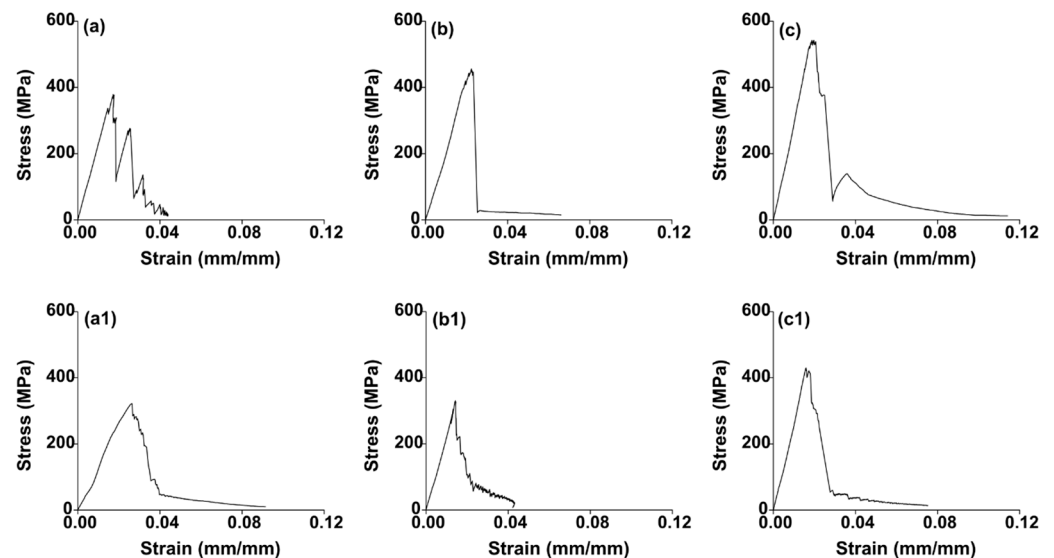
Figure 5. The stress versus strain data plots for the Kevlar/PVB specimens with: (**a**) no nanoparticles, (**b**) 1 wt.% TiO_2, and (**c**) 2 wt.% TiO_2 nanoparticles; and the immersed ones with: (**a1**) no nanoparticles, (**b1**) 1 wt.% TiO_2, and (**c1**) 2 wt.% TiO_2 nanoparticles.

Figure 6 shows the SEM images of the specimens following the tensile tests. The wet Kevlar composite specimens have larger fibers with a rougher surface due to the remaining moisture (images b and d in Figure 6). It can be seen that the wet fibers also coalesced among themselves because of the residual moisture [35].

3.4. Bending Test Results

All the specimens were slightly bent in the middle during the bending test due to the high-modulus Kevlar fibers. The flexural properties such as flexural stress and flexural strain were determined in accordance with the ASTM D 790-03 standard. In order to compare the specimens, the strength was defined as the value of normal stress at a strain of 0.05. However, some of the specimens showed a slight softening of the material before the 5% strain, followed by delayed strengthening, as shown in Figure 7. According to the standard, the strength of the specimens could also be defined as the stress at the local extreme prior to the 5% strain; nonetheless, this would make it impossible to compare them. The tangent modulus of elasticity was used to estimate the flexural modulus through the process of drawing a tangent with the largest slope in the first elastic region of the stress–strain plot. Contrary to the results of the tensile test, the dry
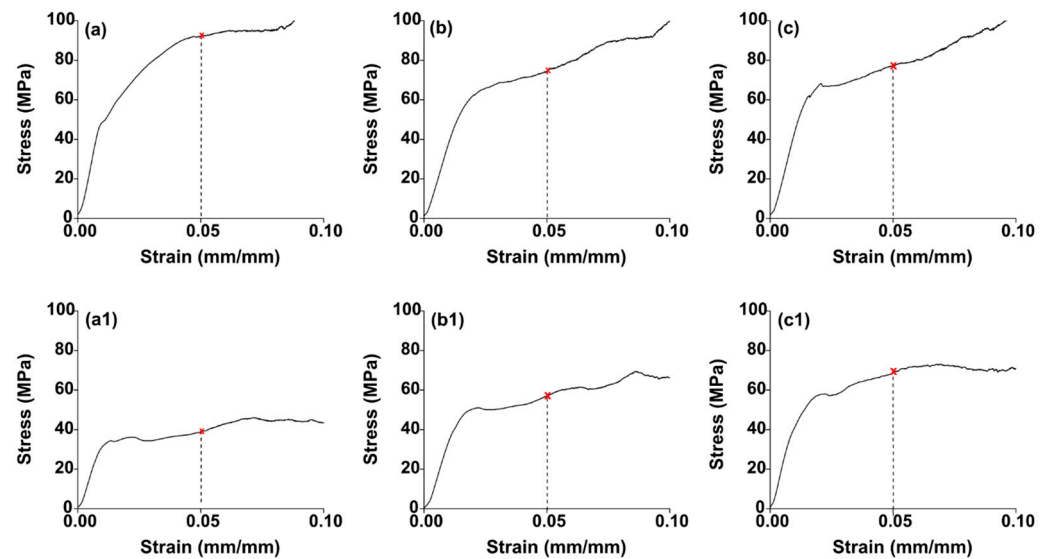
specimens with no nanoparticles had the best flexural strength and modulus because of the improved bonding between their two impregnated layers while the existence of the TiO_2 nanoparticles resulted, to some extent, in the breakage of the shear bond between the layers [36]. Table 2 presents the middle value of the flexural strength at 5% strain for the untreated Kevlar/PVB specimens as 26.2% and 27.5% higher compared to the Kevlar/PVB/1% TiO_2 and Kevlar/PVB/2% TiO_2 specimens, respectively. In comparison with the composites containing 1 wt.% and 2 wt.% TiO_2 nanoparticles, the dry Kevlar/PVB composites set a higher flexural modulus value of 29.1% and 34.0%, correspondingly. The data obtained were also subjected to the coefficient of variation (CoV). Satisfactory values for the CoV can also be considered for the flexural strength, where they range from 5% to 19%. The least reliable results were determined from the stress–strain test diagrams. Significant variability characterizes these diagrams, which is also reflected in the CoV for the flexural modulus (up to 37%).
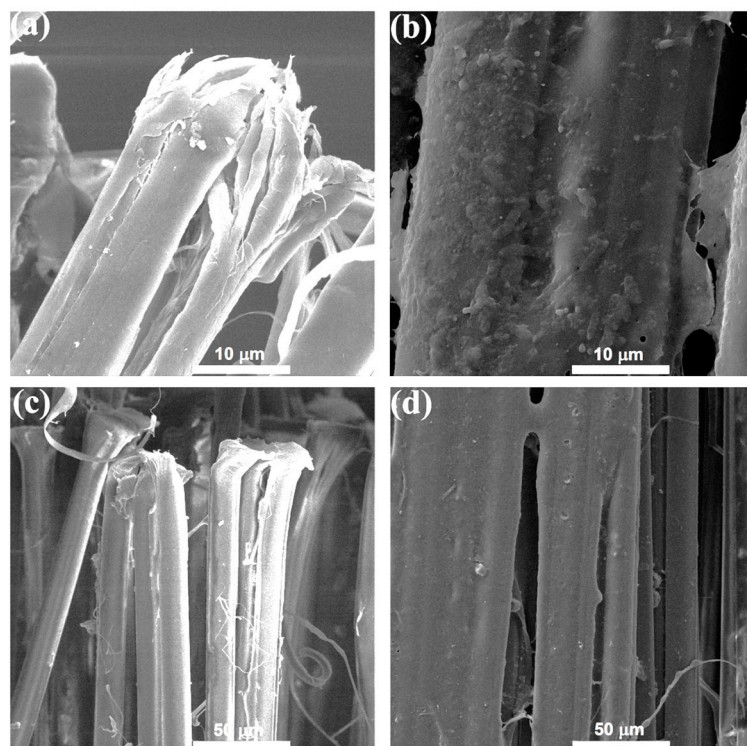
Figure 6. The electron microscope images of: (**a**) dry and (**b**) wet Kevlar/PVB/1% TiO_2 specimens (scale bar 10 μm); and (**c**) dry and (**d**) wet Kevlar/PVB/2% TiO_2 specimens (scale bar 50 μm).

When composite materials are subjected to the liquid medium, their mechanical characteristics deteriorate because the liquid acts as a plasticizer [37]. The reduction in flexural characteristics is attributed to the plasticizing impact of water, as well as the matrix swelling and hydrolysis [38]. The bending property values of all the submerged Kevlar/PVB composite specimens were lower than those of their dry counterparts. The immersed Kevlar/PVB specimens showed the greatest reduction in bending strength at 5% strain, which was 61.4% less than for the dry Kevlar/PVB specimens, as presented in Table 2 and Figure 7. This outcome demonstrated that the absorbed water content was the primary cause of the deterioration of the PVB matrix as a layer in between, which decreased the flexural strength of the specimens. Numerous investigations have demonstrated that PVB is water-sensitive [20,39]. However, the flexural strength of the immersed specimens with the TiO_2 reinforcement did not significantly decrease since nanofillers often enhance the mechanical properties of composite materials in wet conditions (Table 2, Figure 7) [33].

Figure 7. The flexural stress versus strain data plots for the Kevlar/PVB specimens with: (**a**) no nanoparticles, (**b**) 1 wt.% TiO_2, and (**c**) 2 wt.% TiO_2 nanoparticles; and the immersed ones with: (**a1**) no nanoparticles, (**b1**) 1 wt.% TiO_2, and (**c1**) 2 wt.% TiO_2 nanoparticles.

Table 2. The bending test results.

Specimen	Flexural Strength, 5% Strain (MPa)	Flexural Modulus (GPa)
Kevlar/PVB—dry	98.58 ± 4.99	5.61 ± 0.89
Kevlar/PVB—wet	38.02 ± 2.11	4.40 ± 0.62
Kevlar/PVB/1% TiO_2—dry	72.76 ± 5.00	3.98 ± 0.20
Kevlar/PVB/1% TiO_2—wet	45.62 ± 8.44	3.50 ± 1.29
Kevlar/PVB/2% TiO_2—dry	71.45 ± 10.65	3.70 ± 1.13
Kevlar/PVB/2% TiO_2—wet	54.96 ± 9.99	3.01 ± 1.06

3.5. Numerical Modelling

The results of the bending test were used to simulate the bending test in the Abaqus software (v2021). During the simulation, the specimen was bent and the vertical reaction force was recorded (see Figure 8). The Poisson coefficient $v = 0.25$ and the friction coefficient $f = 0.15$ were used in the same way as in [40] where the Kevlar/PVB specimens were also subjected to the three-point bending test. Due to the relatively large deformations (related to the size of the tested specimen), the simulation is defined as 'nonlinear' which allows us to consider the second-order effects. The simulation was driven by displacement, divided into 20 separate steps, each with a displacement magnitude equal to 0.75 mm. The mesh of the tested specimen was made of C3D20R elements (twenty-node brick elements with reduced integration).
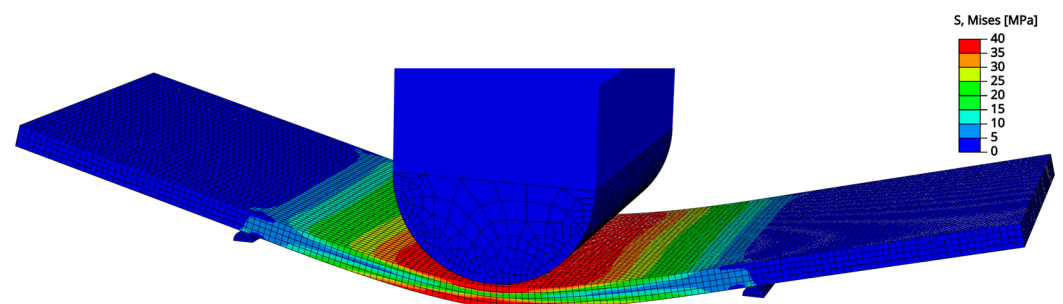
Figure 8. The deformed specimen from the Abaqus simulation with the von Mises stress distribution in megapascals (MPa).

The aim of this numerical model is to understand the experimentally obtained data in detail, and to check the applicability of the approach from the ASTM D 790-03 for the evaluation of the experimental results. Therefore, the standard was used to calculate the values of stress in the outer fibers at the midpoint (Equation (2)), flexural strain (Equation (3)) and tangent modulus of elasticity (Equation (4)). After that, a relevant material model in Abaqus was calibrated to reach an agreement between the results obtained by the numerical simulation and by the experimental testing of the dry specimen 2b—Kevlar/PVB/1% TiO_2.

The standard recommends that we calculate the stress in the outer fibers at midpoint σ_f as:

$$\sigma_f = \left(3PL/2bd^2\right) \cdot \left[1 + 6(D/L)^2 - 4(d/L)(D/L)\right] \tag{2}$$

where P is the load at a given point on the load-deflection curve in [N], L is the support span in [mm], b is the width of the beam tested in [mm], d is the depth of the beam tested in [mm], and D is the deflection of the centerline of the specimen at the middle of the support span in [mm]. The stress σ_f is in [MPa].

The flexural strain ε_f is calculated according to the standard as:

$$\varepsilon_f = 6Dd/L^2 \tag{3}$$

The tangent modulus of elasticity E_B is calculated according to the standard as:

$$E_B = L^3 m/4bd^3 \tag{4}$$

where m is the slope of the tangent to the initial straight-line portion of the load-deflection curve in [N/mm] of deflection.

The linear part of the load-deflection curve has been assumed to be the part with displacement D greater than 0.48 mm and smaller than 0.95 mm, which corresponds to the applied force P greater than 7.90 N and less than 17.90 N, as shown in Figure 9. According to Equation (4), the tangent modulus of elasticity E_B is equal to 4 GPa, since the slope of the linear part of the load-deflection curve m is calculated as $(17.90 - 7.90)$ N$/(0.95 - 0.48)$ mm = 20.4 N/mm, the span between the supports L is 25.0 mm, the width of the tested beam b is 15.0 mm, and the depth of the tested beam d is 1.10 mm. According to Equation (3), the flexural strain ε_f is equal to 0.005 when displacement D is 0.48 mm, and ε_f is equal to 0.010 when D is 0.95 mm. According to Equation (2), the stress in the outer fibers at midpoint σ_f is equal to 16.3 MPa when D is 0.48 mm and P is 7.90 N. When D is 0.95 mm and P is 17.90 N, then σ_f is equal to 37.1 MPa.
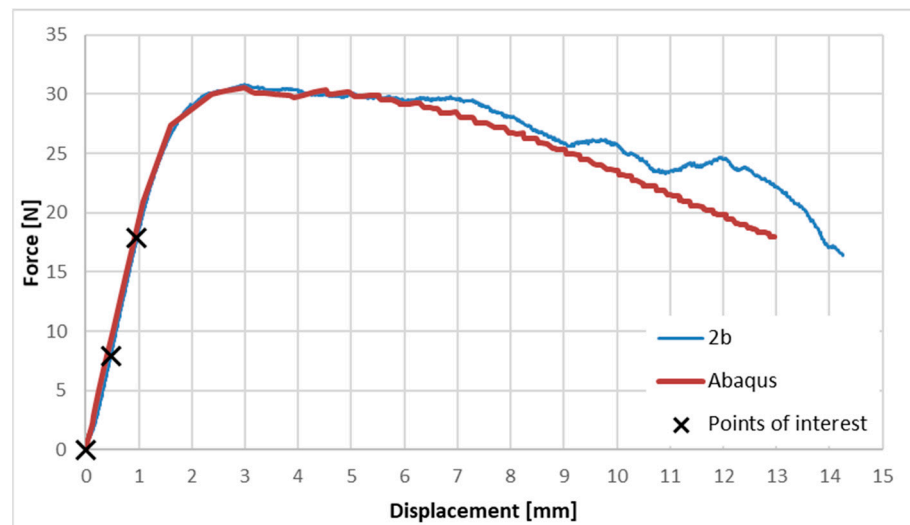
Figure 9. Force-to-displacement curves obtained by Abaqus (red) and experimental testing (blue). Points of interest ($\times$) were used to calculate the inputs for the Abaqus simulation.

These calculated values of stress in the outer fibers at the midpoint (σ_f), flexural strain (ε_f), and tangent modulus of elasticity (E_B) were applied in the Abaqus software in the following way: The tangent modulus of elasticity E_B was used as the modulus of elasticity for the specimen. The plastic component of strain ε_p was calculated by using Hooke's law as follows: $\varepsilon_p = \varepsilon_f - \sigma_f/E_B = 0.010 - (37.1 \text{ MPa})/(4 \text{ GPa}) = 0.000725$. This result (together with the previously calculated values of σ_f equal to 16.3 MPa and 37.1 MPa) was used in the "Yield Stress to Plastic Strain" table in Abaqus. This means that the irreversible plastic behavior starts in the bent specimen when the stress reaches 16.3 MPa and the perfect plasticity (yielding) occurs when the stress reaches 37.1 MPa.

The agreement between both of the results shown in Figure 9 indicates that the simplified definition of the material properties which was used in Abaqus may lead to a successful simulation of a three-point bending test of the Kevlar/PVB composite. It might also indicate that the strain in the outer fibers at the midpoint of the tested specimen was not greater than 1%.

The numerical simulation might also be used to estimate the criterion of applicability of Equation (2) from the ASTM D 790-03 standard to calculate the stress in the outer fibers at midpoint σ_f. In this particular case, it seems to be applicable only until displacement D is less than 0.95 mm. Beyond this value, displacement D may not be considered as a relatively small one, and using Equation (2) from the standard may lead to an overestimated value of the stress σ_f which is greater than 37.1 MPa.

4. Conclusions

In this research, the impact of water immersion and TiO_2 nanoparticles on the mechanical characteristics of Kevlar/PVB composites has been evaluated. The tensile and bending properties of the dry Kevlar/PVB composites were compared with those that had been water-immersed for duration of 8 weeks. The specimens did not completely fracture during the tensile or bending test.

Adding 2 wt.% TiO_2 nanoparticles produced a 39.8% and 24.3% increase in the tensile strength and modulus, respectively, of the untreated Kevlar/PVB specimens without TiO_2 reinforcement. In contrast to this trend of the results, the highest flexural modulus and bending strength were achieved by the dry Kevlar/PVB specimens without nanoparticles as a result of the stronger connection between their two impregnated fabric layers. Compared to their dry counterparts, the tensile and bending properties of every wet specimen resulted in lower values.

There was a nearly complete agreement between the experimentally obtained results and the results from the numerical simulation. This agreement shows that the approach used in the Abaqus software is applicable in order to accomplish a successful simulation of a three-point bending test of the Kevlar/PVB composite.

The acquired results provide crucial information on the effect of water aging on the examined composites. Despite their mechanical degradation, the wet composite specimens retained satisfactory values in terms of tensile strength and tensile modulus.

In this study, the following conclusions can be drawn:

- The addition of TiO_2 nanoparticles improved the tensile properties of Kevlar/PVB composites;
- The immersion process lowered the tensile and bending strength;
- The numerical simulation might provide more realistic values for the stress in the outer fibers at midpoint compared to the analytical formulae of the ASTM D 790-03 standard.

Author Contributions: Conceptualization, V.O., K.V.M. and M.V.; methodology, V.O., M.V. and P.S.; software, P.S.; investigation, V.O., M.V. and A.Z.; writing—original draft preparation, V.O. and P.S.; writing—review and editing, K.V.M. and A.Z. All authors have read and agreed to the published version of the manuscript.

Conflicts of Interest: The authors declare no conflict of interest.

References

1. Seretis, G.V.; Kostazos, P.K.; Manolakos, D.E.; Provatidis, C.G. On the mechanical response of woven para-aramid protection fabrics. *Compos. Part B Eng.* **2015**, *79*, 67–73. [CrossRef]
2. Obradović, V.; Simić, D.; Sejkot, P.; Machalická, K.V.; Vokáč, M. Moisture absorption characteristics and effects on mechanical properties of Kolon/epoxy composites. *Curr. Appl. Phys.* **2021**, *26*, 16–23. [CrossRef]
3. Singh, T.J.; Samanta, S. Characterization of Kevlar fiber and its composites: A review. *Mater. Today Proc.* **2015**, *2*, 1381–1387. [CrossRef]
4. Zhao, Y.; Li, X.; Shen, J.; Gao, C.; Van der Bruggen, B. The potential of Kevlar aramid nanofiber composite membranes. *J. Mater. Chem. A* **2020**, *8*, 7548–7568. [CrossRef]
5. Almaroof, A.; Ali, A.; Mannocci, F.; Deb, S. Semi-interpenetrating network composites reinforced with Kevlar fibers for dental post fabrication. *Dent. Mater. J.* **2019**, *38*, 511–521. [CrossRef] [PubMed]
6. Obradović, V.; Simić, D.; Zrilić, M.; Stojanović, D.B.; Uskoković, P.S. Novel hybrid nanostructures of carbon nanotube/fullerene-like tungsten disulfide as reinforcement for aramid fabric composites. *Fibers Polym.* **2021**, *22*, 528–539. [CrossRef]
7. Kumar, P.; Khan, N.; Kumar, D. Polyvinyl butyral (PVB), versetile template for designing nanocomposite/composite materials: A review. *Green Chem. Technol. Lett.* **2016**, *2*, 185–194. [CrossRef]
8. Obradović, V.; Stojanović, D.B.; Jokić, B.; Zrilić, M.; Radojević, V.; Uskoković, P.S.; Aleksić, R. Nanomechanical and anti-stabbing properties of Kolon fabric composites reinforced with hybrid nanoparticles. *Compos. Part B Eng.* **2017**, *108*, 143–152. [CrossRef]
9. Ismail, I.N.; Ishak, Z.A.M.; Jaafar, M.F.; Omar, S.; Zainal Abidin, M.F.; Ahmad Marzuki, H.F. Thermomechanical properties of toughened phenolic resol resin. *Solid State Sci. Technol.* **2009**, *17*, 155.
10. Grębowski, K.; Wróbel, A. Architectural and Urban Planning Solutions for the Protection of Heritage Buildings in the Context of Terrorist Attacks: Following the Example of Passive Protection Systems. *Buildings* **2022**, *12*, 988. [CrossRef]
11. Mowital—Your Global Partner for PVB. Available online: https://www.kuraray.eu/products-solutions/polyvinyl-butyral (accessed on 27 November 2023).
12. Hooper, A.; Blackman, B.R.K.; Dear, J.P. The mechanical behaviour of poly (vinyl butyral) at different strain magnitudes and strain rates. *J. Mater. Sci.* **2012**, *47*, 3564. [CrossRef]
13. Sánchez, M.; Campo, M.; Jiménez-Suárez, A.; Ureña, A. Effect of the carbon nanotube functionalization on flexural properties of multiscale carbon fiber/epoxy composites manufactured by VARIM. *Compos. Part B Eng.* **2013**, *45*, 1613–1619. [CrossRef]
14. Mhadhbi, M.; Abderazzak, H.; Avar, B. *Synthesis and Properties of Titanium Dioxide Nanoparticles*; Intechopen: London, UK, 2023; Available online: https://www.intechopen.com/chapters/87015 (accessed on 10 January 2024).
15. Siwińska-Stefańska, K.; Jesionowski, T. Advanced hybrid materials based on titanium dioxide for environmental and electrochemical applications. In *Titanium Dioxide*; IntechOpen: London, UK, 2017; Available online: https://www.intechopen.com/chapters/55832 (accessed on 10 January 2024).
16. Nawaz, H.; Umar, M.; Maryam, R.; Nawaz, I.; Razzaq, H.; Malik, T.; Liu, X. Polymer Nanocomposites based on TiO_2 as a reinforcing agent: An Overview. *Adv. Eng. Mater.* **2022**, *24*, 2200844. [CrossRef]
17. Zamanian, M.; Sadrnia, H.; Khojastehpour, M.; Hosseini, F.; Thibault, J. Effect of TiO_2 nanoparticles on barrier and mechanical properties of PVA films. *J. Membr. Sci. Res.* **2021**, *7*, 67–73.
18. Amit, C.; Islam, M.S. Fabrication and characterization of TiO_2-epoxy nanocomposites. *Mater. Sci. Eng. A* **2008**, *487*, 574–585.
19. Doxsee JR, L.E.; Janssens, W.; Verpoest, I.; De Meester, P. Strength of aramid-epoxy composites during moisture absorption. *J. Reinf. Plast. Comp.* **1991**, *10*, 645–655. [CrossRef]
20. Desloir, M.; Benoit, C.; Bendaoud, A.; Alcouffe, P.; Carrot, C. Plasticization of poly (vinyl butyral) by water: Glass transition temperature and mechanical properties. *J. Appl. Polym. Sci.* **2019**, *136*, 47230. [CrossRef]
21. Botelho, E.C.; Silva, R.A.; Pardini, L.C.; Rezende, M.C. A review on the development and properties of continuous fiber/epoxy/aluminum hybrid composites for aircraft structures. *Mater. Res.* **2006**, *9*, 247–256. [CrossRef]
22. *ISO 62:2008*; Plastics—Determination of Water Absorption. ISO (International Organization for Standardization): Geneva, Switzerland, 2008.
23. Obradović, V.; Bajić, D.; Sejkot, P.; Fidanovski, B.; Machalická, K.V.; Vokáč, M. Effect of moisture absorption on the thermomechanical properties of carbon/epoxy composites with SiC reinforcement. *Compos. Interfaces* **2022**, *29*, 1309–1324. [CrossRef]
24. *ASTM D3039/D3039M-08*; Standard Test Method for Tensile Properties of Polymer Matrix Composite Materials. ASTM International: West Conshohocken, PA, USA, 2008.
25. *ASTM D790-03*; Standard Test Methods for Flexural Properties of Unreinforced and Reinforced Plastics and Electrical Insulating Materials. ASTM International: West Conshohocken, PA, USA, 2003.
26. Alamri, H.; Low, I.M. Effect of water absorption on the mechanical properties of nano-filler reinforced epoxy nanocomposites. *Mater. Des.* **2012**, *42*, 214–222. [CrossRef]

27. Alamri, H.; Low, I.M. Effect of water absorption on the mechanical properties of n-SiC filled recycled cellulose fibre reinforced epoxy eco-nanocomposites. *Polym. Test.* **2012**, *31*, 810–818. [CrossRef]
28. Obradović, V.; Vuksanović, M.; Tomić, N.; Petrović, M.; Marinković, A.; Stojanović, D.; Radojević, V.; Heinemann, R.J.; Uskoković, P. Impact properties of Kolon/PVB fabrics reinforced with rice-husk silica particles. *Mater. Lett.* **2022**, *324*, 132668. [CrossRef]
29. Ehrhart, B.; Valeske, B.; Ecault, R.; Boustie, M.; Berthe, L.; Bockenheimer, C. Extended NDT for the quality assessment of adhesive bonded CFRP structures. In Proceedings of the Smart Material, Structures & NDT in Aerospace Conference, Montreal, QC, Canada, 2 November 2011.
30. Callister, W.D., Jr. *Materials Science and Engineering: An Introduction*, 7th ed.; John Wiley & Sons, Inc.: New York, NY, USA, 2007.
31. Fu, S.Y.; Feng, X.Q.; Lauke, B.; Mai, Y.W. Effects of particle size, particle/matrix interface adhesion and particle loading on mechanical properties of particulate–polymer composites. *Compos. Part B-Eng.* **2008**, *39*, 933–961. [CrossRef]
32. Wang, M.; Berry, C.; Braden, M.; Bonfield, W. Young's and shear moduli of ceramic particle filled polyethylene. *J. Mater. Sci. Mater. Med.* **1998**, *9*, 621–624. [CrossRef]
33. Al-Maharma, A.Y.; Al-Huniti, N. Critical review of the parameters affecting the effectiveness of moisture absorption treatments used for natural composites. *J. Compos. Sci.* **2019**, *3*, 27. [CrossRef]
34. Akay, M.; Mun, S.K.; Stanley, A. Influence of moisture on the thermal and mechanical properties of autoclaved and oven-cured Kevlar-49/epoxy laminates. *Compos. Sci. Technol.* **1997**, *57*, 565–571. [CrossRef]
35. Ahn, H.; Wee, J.H.; Kim, Y.M.; Yu, W.R.; Yeo, S.Y. Microstructure and Mechanical Properties of Polyacrylonitrile Precursor Fiber with Dry and Wet Drawing Process. *Polymers* **2021**, *13*, 1613. [CrossRef] [PubMed]
36. Ogrodowska, K.; Łuszcz, K.; Garbacz, A.N. Hybridization and Temperature Impact on Shear Strength of Basalt Fiber-Reinforced Polymer Bars. *Polymers* **2021**, *13*, 2585. [CrossRef]
37. Somaiah Chowdary, M.; Raghavendra, G.; Niranjan Kumar, M.S.R.; Ojha, S.; Om Prakash, M. A review on the degradation of properties under the influence of liquid medium of hybrid polymer composites. *SN Appl. Sci.* **2020**, *2*, 1708. [CrossRef]
38. Rafiq, A.; Merah, N. Nanoclay enhancement of flexural properties and water uptake resistance of glass fiber-reinforced epoxy composites at different temperatures. *J. Compos. Mater.* **2019**, *53*, 143–154. [CrossRef]
39. Tupý, M.; Měřínská, D.; Svoboda, P.; Kalendová, A.; Klásek, A.; Zvoníček, J. Effect of water and acid–base reactants on adhesive properties of various plasticized poly (vinyl butyral) sheets. *J. Appl. Polym. Sci.* **2013**, *127*, 3474–3484. [CrossRef]
40. Hou, P.; Zhao, H.; Ma, Z.; Zhang, S.; Li, J.; Dong, X.; Sun, Y.; Zhu, Z. Influence of punch radius on elastic modulus of three-point bending tests. *Adv. Mech. Eng.* **2016**, *8*, 1–8. [CrossRef]